nature chemistry

ARTICLES

https://doi.org/10.1038/s41557-019-0330-x

Identification of a Frank–Kasper Z phase from shape amphiphile self-assembly

Zebin Su[1,2], Chih-Hao Hsu[2], Zihao Gong[2], Xueyan Feng[2], Jiahao Huang[2], Ruimeng Zhang[2], Yu Wang[2], Jialin Mao[2], Chrys Wesdemiotis[2], Tao Li[3,4], Soenke Seifert[3], Wei Zhang[1], Takuzo Aida[5,6], Mingjun Huang[1*] and Stephen Z. D. Cheng[1,2*]

Frank–Kasper phases, a family of ordered structures formed from particles with spherical motifs, are found in a host of materials, such as metal alloys, inorganic colloids and various types of soft matter. All the experimentally observed Frank–Kasper phases can be constructed from the basic units of three fundamental structures called the A15, C15 and Z phases. The Z phase, typically observed in metal alloys, is associated with a relatively large volume ratio between its constituents, and this constraint inhibits its formation in most self-assembled single-component soft-matter systems. We have assembled a series of nano-sized shape amphiphiles that comprise a triphenylene core and six polyhedral oligomeric silsesquioxane cages grafted onto it through linkers to give a variety of unconventional structures, which include the Z phase. This structure was obtained through fine tuning of the linker lengths between the core and the peripheral polyhedral oligomeric silsesquioxane cages, and exhibits a relatively large volume asymmetry between its constituent polyhedral particle motifs.

Humans have continued to explore microscopic structures of matter. Spherical assemblies, deceptively simple structures, occur in various materials from metal alloys and inorganic colloids to assembled soft matters[1]. Ubiquitous densely packed structures—such as face-centred cubic, hexagonal close-packed and body-centred cubic (BCC) structures—are formed in the majority of metallic elements. Three decades ago, the discovery of quasicrystal expanded the list of crystal classifications from 230 space group symmetry to infinity[2]. Between the cases of ordered but non-periodic quasicrystal, and simple densely packed structures (for example, face-centred cubic, hexagonal close-packed and BCC), there is a class of metal alloy crystal structures, so-called Frank–Kasper (FK) phases[3,4]. FK phases are topologically close-packed and contain exclusively tetrahedral interstices composed of a polyhedron with coordination number CN = 12 and at least one polyhedron with higher CN (CN = 14, 15 or 16) (Fig. 1a). Often, FK phases can be viewed as ordered approximates of quasicrystal phases due to some shared construction rules from sphere packing[5–7]. So far, 27 different types of FK phases have been found experimentally[8].

To better understand the relationship between these FK phase structures, we can express all the 27 observed FK phase structures by a scheme of $(R_3X)_i(PX_2)_j(Q_2R_2X_3)_k$ (i, j and k are non-negative integers) in which X, P, Q and R represent CN = 12, 16, 15 and 14, respectively (Supplementary Table 1), of FK polyhedra[9]. For example, R_3X represents an A15 phase, PX_2 represents a Laves C15 phase (can also be a C14 or C36 phase) and $Q_2R_2X_3$ represents a Z phase. These A15, C15 and Z phases adopt three fundamental structures that provide the basic units to construct all the other FK phases so far reported. If we plot a relationship between the average coordination number and the fraction of CN = 15 polyhedra in a FK phase, all these 27 FK phases are located in a triangle with the three basic FK phases located at three vertices (Fig. 1b)[9]. Ordered assemblies that are isostructural to these three basic FK phases have been identified in diverse systems, which include natural clathrate hydrates in which the host molecule is water and the guest molecule is typically a gas, such as methane[10], zeolites, which are hydrated microporous aluminosilicate minerals[11], and clathrate colloidal crystals directed by a DNA-programmable assembly[12].

The first FK phase in soft matter, A15 (space group $Pm\bar{3}\ n$), was reported in 1992 in lipid-containing micelle systems[13,14] and further demonstrated in subsequent studies of the bulk self-assembly of single component soft matter systems[15,16]. Subsequently, several FK phases and dodecagonal quasicrystals were also identified in dendrimers[17–20], block copolymers[21,22], concentrated ionic surfactants[23,24] and giant molecules[25,26]. Recently, the C14 phase (space group $P6_3/mmc$) and the C15 phase (space group $Fd\bar{3}\ m$) in a metastable state were reported in diblock copolymers by Bates and co-workers in 2017[27,28]. However, despite these extensive works, to the best of our knowledge, the Z phase (space group $P6/mmm$) remains the only one of the three fundamental structures for the 27 discovered FK phases that has not been observed in any soft matter system. Experimental demonstration of the Z phase would not only provide insight on the structure and formation mechanism of such phases, but also perhaps help guide the construction of more complicated FK phases in soft matter.

The self-assembly of giant molecules is a powerful platform to create diverse structures in soft matter because their primary stereochemistry, composition, chemical sequence, molecular topology and molecular weight can be precisely controlled[25,26,29,30]. Furthermore, specific intra- and/or intermolecular interactions can be rationally incorporated in the molecules by accurate design and synthesis. In a single-component soft matter system, FK phases

[1]South China Advanced Institute for Soft Matter Science and Technology, School of Molecular Science and Engineering, South China University of Technology, Guangzhou, China. [2]Department of Polymer Science, College of Polymer Science and Polymer Engineering, University of Akron, Akron, OH, USA. [3]X-ray Science Division, Advanced Photon Source, Argonne National Laboratory, Argonne, IL, USA. [4]Department of Chemistry and Biochemistry, Northern Illinois University, DeKalb, IL, USA. [5]Department of Chemistry and Biotechnology, School of Engineering, The University of Tokyo, Tokyo, Japan. [6]Riken Center for Emergent Matter Science, Wako, Saitama, Japan. *e-mail: huangmj25@scut.edu.cn; scheng@uakron.edu

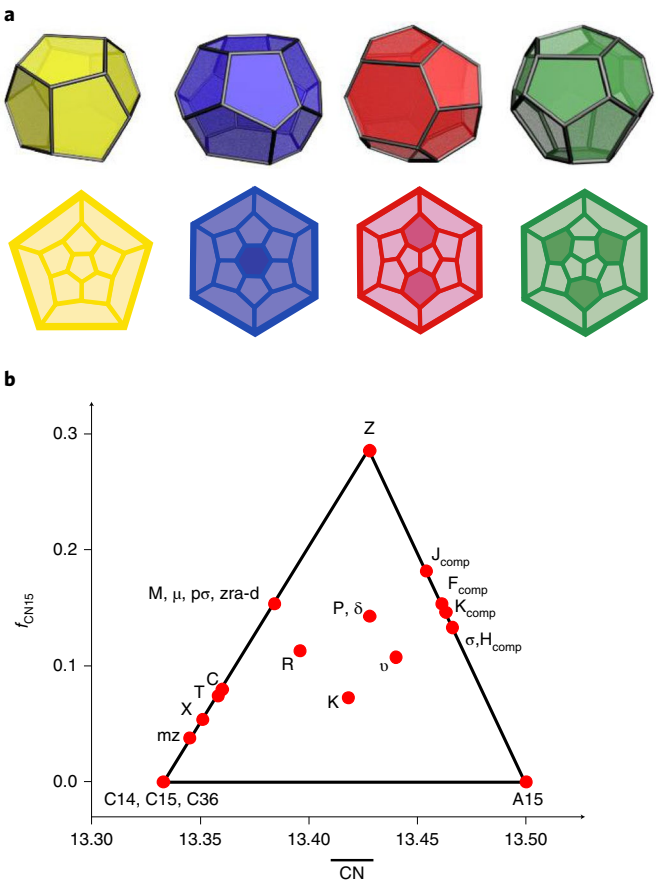

Fig. 1 | FK polyhedra and phases. a, Three-dimensional models and planar graphs of FK polyhedra. Yellow polyhedron: CN = 12; blue polyhedron: CN = 14; red polyhdron: CN = 15; green polyhedron: CN = 16. **b**, The triangle includes all the FK phases experimentally observed so far, with C15, A15 and Z located at the three vertices of triangle. The horizontal axis is the average CN and the vertical axis is the fraction of polyhedra with CN = 15. Comp, complex.

are self-assembled through a hierarchical organization process in which molecules first assemble into spherical motifs. During the phase formation, these spherical motifs go through a process of deforming, or 'squishing', to form polyhedra (Wigner–Seitz cells or, as referred to here, Voronoi cells) and fill voids in the FK lattices. In addition, variation of the numbers of molecules in each polyhedron is understood to be a factor for the size heterogeneity of the polyhedra. Most FK phases driven by phase segregation possess volume asymmetry, here defined as the volume asymmetry ratio of the largest and the smallest Voronoi cells. The A15 and σ phases possess relatively small volume asymmetry ratios of 1.03 and 1.17, respectively[27,31], which could be the reason why only these two FK phases have been frequently observed in soft matter. In contrast, in the C14 and C15 phases, the volume asymmetry ratio reaches over 1.20, which renders C14 and C15 very scarce phases in soft matter[23,27]. The Z phase usually requires a comparably large volume asymmetry ratio (>1.20)[27,31]. However, it also requires a mean coordination number (13.428) much larger than those of the C14 and C15 (both are 13.333) phases. The polyhedral motifs induced by the deformation of soft spherical particles, used to access other FK phases, may not be suitable to achieve the relatively large volume asymmetry ratio and high coordination number required by a Z phase. A new molecular design is thus necessary to promote this particular packing of spherical motifs in FK polyhedra.

Here we designed and synthesized a series of nanosized shape amphiphiles in which a triphenylene core is attached to six identical polyhedral oligomeric silsesquioxane (POSS) cages at the periphery through covalent linkers with tunable lengths (Fig. 2). Shape amphiphiles are molecular building blocks that consist of different moieties of distinct shapes, and engage in competing interactions[32,33]. The relatively weak π–π stacking interactions among conjugated aromatic triphenylene cores enable the segregation from peripheric BPOSS cages (POSS functionalized with seven isobutyl groups). Owing to the tunable steric hindrance by the rigid and bulky BPOSS cages, these nanosized shape amphiphiles do not self-assemble into a one-dimensional columnar structure, as commonly observed in plate-like molecules[34]. Moreover, the tunability of the linker length enables the formation of various ordered spherical phases. Using this platform, we report the experimental observation of the FK Z phase in a soft matter system.

Results and discussion

Synthesis and characterization. The nanosized shape amphiphiles were synthesized by attaching six bulky BPOSS cages to the triphenylene core through a copper-catalysed azide–alkyne [3 + 2] cycloaddition (CuAAC reaction (Fig. 3. and Supplementary Figs. 1–3)). With this approach, we prepared a series of samples with varied linker lengths that ranged from **Tp-C_0-6BP** to **Tp-C_5-6BP**. The characteristic thermal properties of this set of samples were measured by differential scanning calorimetry (Supplementary Fig. 4). We confirmed π–π stacking interactions between triphenylene units by ultraviolet–visible spectroscopy, consistent with previously reports[19,34] (Supplementary Fig. 5). After thermal annealing, a variety of supramolecular phases were obtained, as demonstrated by a combination of synchrotron small-angle X-ray scattering (SAXS) patterns and bright-field transmission electron microscopy (BFTEM) images.

Analysis of self-assembly behaviour and phase transition. For the nanosized shape amphiphile, **Tp-C_0-6BP**, without a flexible methyl group linker between the phenyl group and the BPOSS cage (Fig. 2b), the quenched sample after annealing at 150 °C exhibited a SAXS pattern with scattering vector q ratios of $\sqrt{2} : \sqrt{4} : \sqrt{5} : \sqrt{6} : \sqrt{8} : \sqrt{10} : \sqrt{13} : \sqrt{14}$ (Fig. 4a), which suggests an A15 phase with a unit cell parameter $a = 6.53$ nm. This structure was further confirmed by a representative 4^4 square tiling pattern along the [001] direction in the BFTEM image and the corresponding fast Fourier transform (FFT) pattern (Fig. 4b and top right inset, respectively). Based on prior crystallographic knowledge, each A15 phase is composed of two CN = 12 polyhedra and six CN = 14 polyhedra at Wyckoff positions 2a and 6c (Fig. 4c), respectively. The volumes of different spherical motifs usually vary by less than ±10% compared with their average value[16,25,31]. The number of **Tp-C_0-6BP** molecules in each A15 unit cell is 32, determined by the unit cell parameters and experimentally measured density. The average number of **Tp-C_0-6BP** molecules in each polyhedron is thus four, as there are a total of eight polyhedra (two types) in the A15 unit cell. Different degrees of deformability of equal-sized spherical motifs may be sufficient to provide enough volume variation to generate the A15 phase.

We next increased the annealing temperature of **Tp-C_0-6BP** to 170 °C. On doing so, a structure transition with a new set of sharp Bragg diffractions and distinctive intensities was observed (Fig. 4d). Analysis showed that this is a Z phase lattice with $a = 6.23$ nm and $c = 6.48$ nm (Supplementary Fig. 6 and Supplementary Table 2), with detailed assignments included in Fig. 4d. The BFTEM images (Fig. 4e,g, and also Fig. 4f,h after Fourier filtering). Their FFT patterns (insets of Fig. 4e,g) from the [001] and [100] directions match well with the simulated projections. All the experimental evidence in both the reciprocal and real spaces confirm the formation of a Z

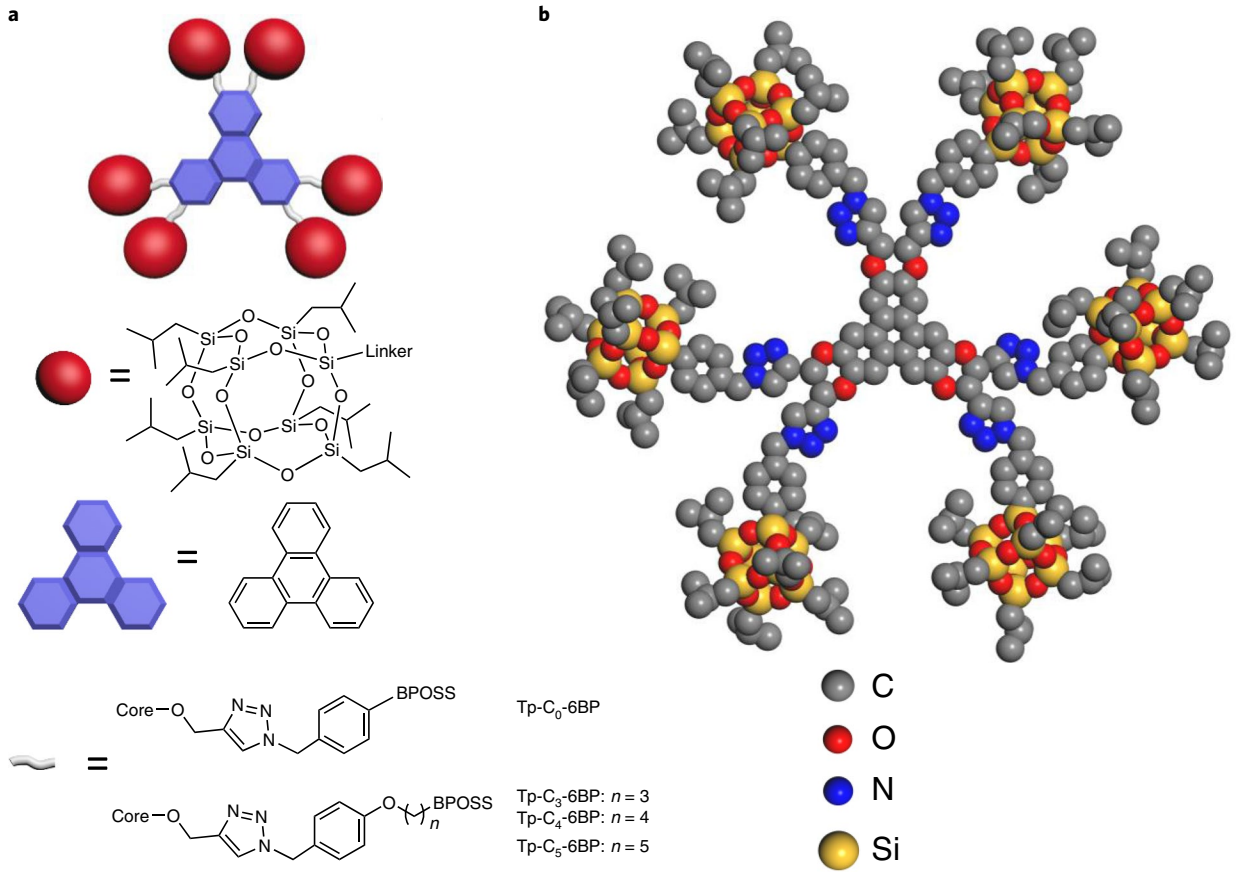

Fig. 2 | Molecular model and chemical structures. a, Schematic representation of a nanosized shape amphiphile, in which the blue disc and red spheres represent the triphenylene core and BPOSS cages, respectively. The chemical structures of the different linkers are also shown, illustrated by grey wavy segments. **b**, The chemical structure of molecule **Tp-C_0-6BP**. Hydrogen atoms are not shown in the molecular model for clarity.

phase. This phase remains thermodynamically stable up to 230 °C, and reaches a disordered melt (Supplementary Fig. 7). It can also form directly from the disordered melt without passing through the low-temperature A15 phase (Supplementary Fig. 8).

We next took the A15 phase sample, generated by annealing at 150 °C, and heated it to 170 °C. On doing so, we observed that the Z phase formed within 12 h (Fig. 5a). When this sample was cooled to 150 °C, the A15 phase was recovered after 7 days (Fig. 5b), which indicates asymmetric phase transition kinetics. Nevertheless, the A15 phase in **Tp-C_0-6BP** is a thermodynamically stable phase in the low-temperature region below 150 °C, a typical enantiotropic phase behaviour[35].

In principle, a Z phase unit cell consists of three CN = 12, two CN = 14 and two CN = 15 polyhedra at Wyckoff positions of 3f, 2e and 2d, respectively (Fig. 4c). According to the Zr_4Al_3 structure, the sizes of CN = 14 and CN = 15 polyhedra are larger than those of CN = 12 polyhedra. For the self-assembled Z phase of **Tp-C_0-6BP**, each unit cell contains approximately 25 molecules determined by the experimentally measured density and unit cell parameters. A probable scenario for the nanosized shape amphiphile system is that each large polyhedron with CN = 14/CN = 15 contains 4 molecules and each small polyhedron with CN = 12 contains 3 molecules. In this case, the volume ratio of the two types of polyhedra is ~1.33, which is within the volume asymmetry ratio range reported in other Z-phase forming systems[31,36]. Although there is no direct evidence of volume asymmetry for the observed Z phase in this work, it is worth noting that previous theories reported volume asymmetry larger than 4:3 for the Z phase[31,36], but not for the A15 phase. This result demonstrates that the balance between the π–π interactions of triphenylene and the steric hindrance of BPOSS cages is a general strategy to reach large volume ratios of FK polyhedra and can be extended to the possible finding of other FK phases.

To study the mechanism of the phase transition between the A15 and Z phases, we further characterized our samples by transmission electron microscopy (TEM). A TEM image illustrates a planar defect with a translation vector $[\sqrt{3}/2, 1/2, 0]$ observed along the [001] direction of the A15 phase (Fig. 6a,b). The square (4^4) tiling pattern corresponds to the A15 unit cell, whereas the regular triangular (3^6) tiling pattern is recognized as the defect in the A15 structure and proposed to be the unit cell of the Z phase (Fig. 6b). Five layers in the A15 unit cell are designated as a sequence of c, b, a, b and c, and in the Z phase unit cell they are denoted as a sequence of A, B, C, B and A (Fig. 6c). The A15 and Z phase unit cells possess identical polyhedra on the A and a planes. Although those polyhedra on the B and C planes do not change their relative positions compared with the b and c plane, respectively, the coordination environment of these positions does change (Fig. 6c): polyhedra on the B plane have CN = 15 (red solid circles) and polyhedra on the b plane have CN = 14 (blue solid circles), polyhedra on the C plane have CN = 12 (yellow empty circles) and polyhedra on the c plane have CN = 14. An analogous mechanism was reported for Cr_3Si and β-tungsten[37,38].

At the molecular level, increasing the temperature weakens the π–π interactions of the cores and strengthens the thermal fluctuation and/or expansion of the bulky BPOSS cages. Most of the columnar phases formed by triphenylenes with alkyl side chains possess a disordered

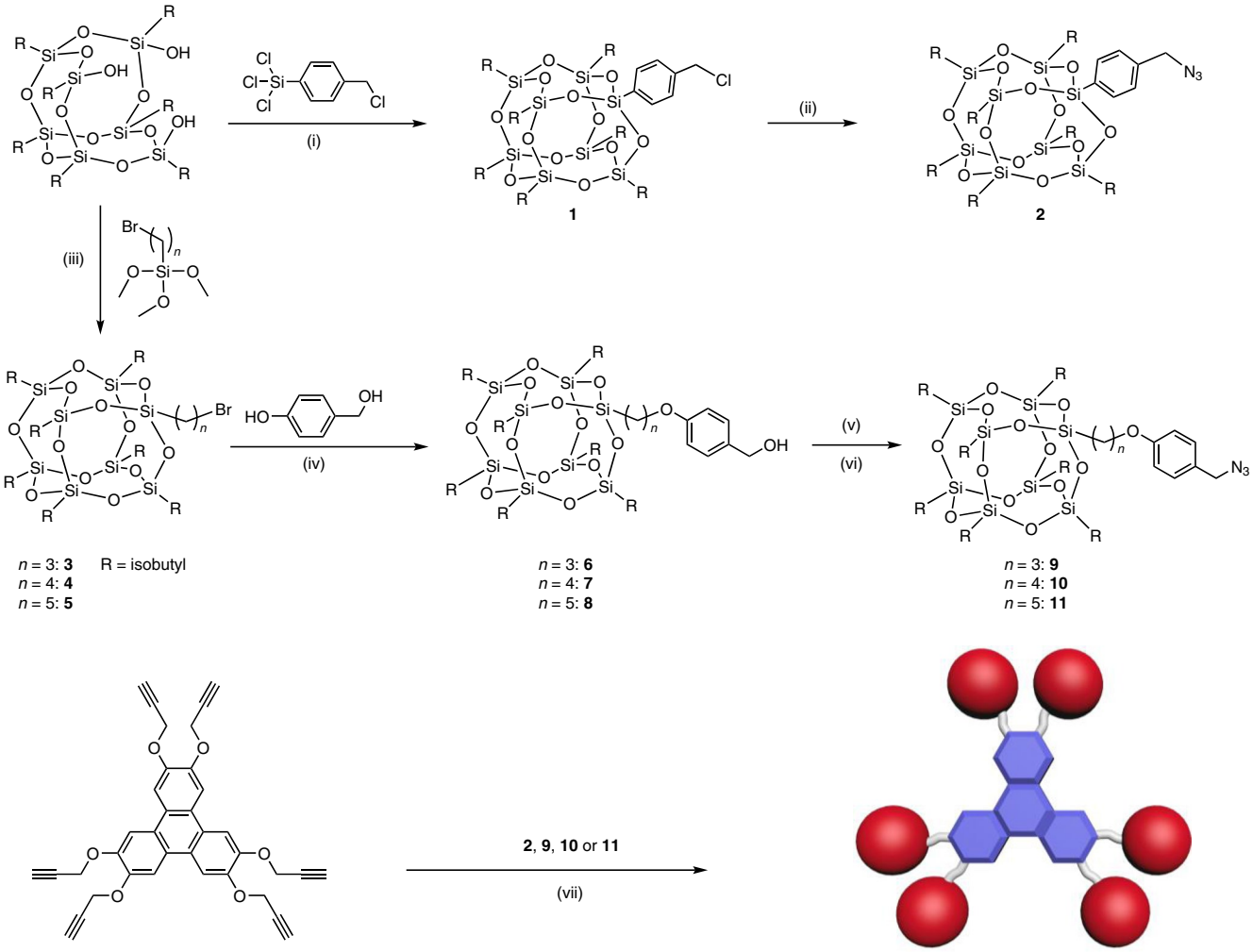

Fig. 3 | Synthesis of the nanosized shape amphiphiles. Reagents and conditions: (i) DBU (1,8-diazabicyclo[5.4.0]undec-7-ene), THF, 25 °C; (ii) NaN_3, THF–DMF (dimethyl formamide), 70 °C; (iii) $N(Et)_4OH$, THF, 25 °C; (iv) DBU, THF–DMF, 70 °C; (v) $SOCl_2$, dichloromethane, 45 °C; (vi) NaN_3, THF–DMF, 70 °C; (vii) CuBr, *N*,*N*,*N*′,*N*′′,*N*′′-pentamethyldiethylenetriamine, THF, 25 °C.

transition that ranges from about 70 °C to over 200 °C, depending on the chemical structure and the side chains[19,34]. This flexibility may facilitate the exchange of nanosized molecules and reorganization among polyhedra in the original A15 phase and enable the redistribution of the polyhedral motifs to form the Z phase.

We next studied the impact of linker length on self-assembly. **Tp-C_3-6BP**, **Tp-C_4-6BP** and **Tp-C_5-6BP** contain relatively flexible alkyl linkers with three, four and five methylene units, respectively, compared to **Tp-C_0-6BP**. After annealing at 170 °C for 12 h, all three samples exhibited SAXS scattering patterns with q ratios of $1:\sqrt{2}:\sqrt{3}:\sqrt{4}$ (Supplementary Fig. 9), consistent with BCC structures and in contrast to that observed with **Tp-C_0-6BP**. The cubic unit cell parameters of **Tp-C_3-6BP**, **Tp-C_4-6BP** and **Tp-C_5-6BP** are $a = 4.78$, 4.88 and 5.04 nm (Supplementary Table 3), which indicates that the mean average radii of the motifs are 2.35, 2.40 and 2.49 nm, respectively. These results further suggest that linker rigidity appears to be crucial to our ability to access the Z phase using these molecules.

Thermodynamic analysis of self-assembly behaviour. Thermodynamically, the driving force of packing supramolecular polyhedra (deformed spherical motifs) into these supramolecular phase structures is to minimize the surface area of the polyhedra contact while filling space with a uniform density[39]. The surface area is inversely proportional to the mean spherical symmetry of the polyhedral motifs in each packing structure. In other words, the polyhedra tend to maximize the spherical symmetry and at the same time to fill the space as efficiently as possible. We quantified the spherical symmetry of the three phases by using the isoperimetric quotient, $IQ = 36\pi V^2/S^3$, where V is the polyhedral volume and S the polyhedral surface area, based on Voronoi cells). Using this metric, a perfect sphere would show a maximum value of 1.0. On average, among the Z phase, A15 and BCC phases, the deviation in the Z phase (IQ = 0.7640) is the least, followed by the A15 phase (IQ = 0.7618) and then the BCC phase (IQ = 0.7534)[27,31]. These values are calculated based on a simplified Voronoi partition with Wyckoff positions as the generating points, which is an approximation for the realistic surface-to-volume ratio or volume asymmetry. The spherical motifs are thus less deformed on average, and have a lower contact surface area in the Z phase, followed by the A15 phase and the most deformed motifs are present in the BCC phase. The **Tp-C_0-6BP** nanosized molecule is relatively rigid and therefore capable of forming highly spherical supramolecular assemblies. As a result, these self-assemble into the Z or A15 phase rather than

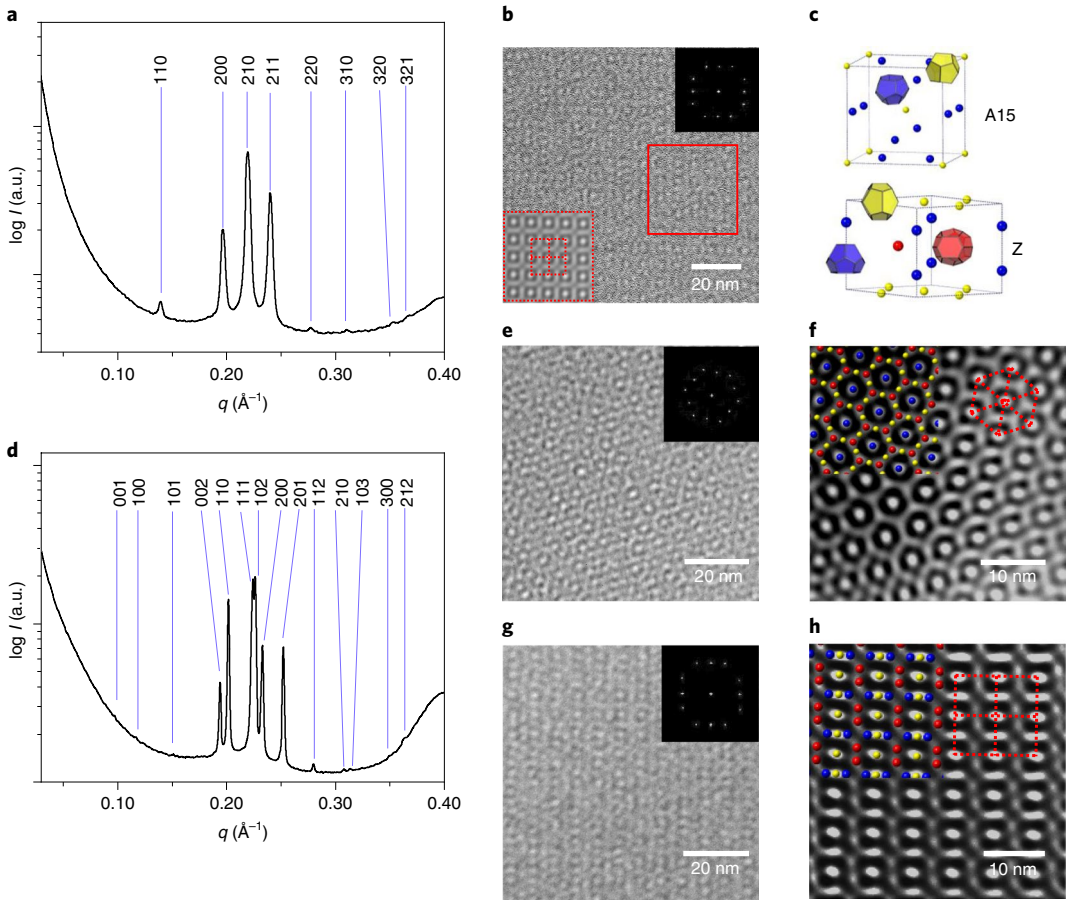

Fig. 4 | Self-assembled structure of Tp-C_0-6BP. a, SAXS pattern of the A15 phase obtained from **Tp-C_0-6BP** after annealing at 150 °C. **b**, TEM image taken along the [001] direction of the A15 phase. Bottom left inset: The Fourier filtered image of the local TEM image marked by red square box. Top right inset: FFT pattern. **c**, Top: the CN = 12 polyhedra (yellow) and CN = 14 polyhedra (blue) locate in the 2a and 6c Wyckoff positions of the A15 phase unit cell, respectively. Bottom: the CN = 12 polyhedra (yellow), CN = 14 polyhedra (blue) and CN = 15 polyhedra (red) locate at the 2d, 2e and 3f Wyckoff positions of the Z phase unit cell, respectively. In crystallography, a Wyckoff position is a point belonging to a set of points that share the same site symmetry and conjugate subgroups of the space group. The Wyckoff positions indicate where the atoms in a crystal can be found. **d**, The SAXS pattern of **Tp-C_0-6BP** after annealing at 170 °C. **e**,**g**, TEM images from the [001] and [100] directions and corresponding FFT patterns (insets) of **Tp-C_0-6BP** after annealing at 170 °C. **f**,**h**, Fourier filtered and magnified images of **e** and **g**, respectively. The insets of **f** and **h** show simulated projection views along the [001] and [100] directions, respectively. a.u., arbitrary units; q, scattering vector; I, scattering intensity.

into the BCC phase. Increasing the temperature enhances the thermal fluctuation and/or expansion of the bulky BPOSS cages, which drives the spherical motifs constructed by the **Tp-C_0-6BP** molecules to be even less deformed. Therefore, with the redistribution capability of the nanosized shape amphiphiles among the motifs, the A15 phase transfers to the Z phase on heating. Maximizing the sphere symmetry decreases the contact surface area, reduces the constraint of the BPOSS cage shell and increases the orientational entropy. Meanwhile, this is well balanced by the relatively high coordination number in the Z phase and so reaches a uniform density in space. In contrast, owing to the relatively flexible linkers in **Tp-C_3-6BP**, **Tp-C_4-6BP** and **Tp-C_5-6BP**, the self-assembled spherical motifs possess a high degree of flexibility and deformability, and the BCC phases with a higher spherical deformation and packing efficiency appear as the thermodynamic stable phase.

Conclusion

In summary, we report the observation of the FK Z phase in a single-component soft material. This phase, together with the A15 and C15 phases (previously observed experimentally[15,16,27,28]), represent the three fundamental structures that provide the building blocks to construct all 27 FK phases discovered. This work also demonstrates a phase transition behaviour from the A15 phase to the Z phase in both reciprocal and real space. Key to this study was the design and synthesis of a series of nanosized shape amphiphiles, in which a triphenylene core was attached with six BPOSS cages at the periphery through covalent linkers with a tunable length. The self-assembly of these nanosized shape amphiphiles results in a variety of highly ordered unconventional supramolecular lattices. This platform presents a feasible method to reach a relatively large volume asymmetry ratio between the assembled motifs. Therefore, ordered phases that include but are not limited to FK phases formed by relatively large volume asymmetry ratios of two or more types of spherical motifs may no longer be out of reach for single-component soft matter.

Methods

Materials, syntheses, characterization data and methods for matrix-assisted laser desorption/ionization–time of flight, differential scanning calorimetry, ultraviolet visible spectroscopy, Fourier filtering and density measurements are described in Supplementary Information.

SAXS measurements. Synchrotron SAXS data are from the 12-ID-B,C station at the Advanced Photon Source of the Argonne National Laboratory. The X-ray energy was 12 KeV. The sample-to-detector distance was adjusted to provide a

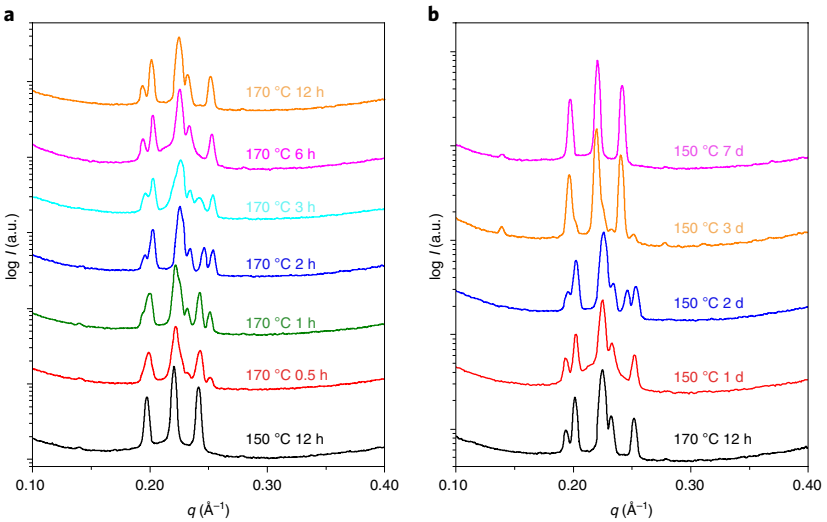

Fig. 5 | Investigations of the phase transition between the A15 phase and the Z phase through SAXS profiles. a, Annealing the completely formed A15 phase of **Tp-C_0-6BP** (profile shown in black) at 170 °C transforms it into the Z phase (orange) within 12 h. **b**, The completely formed Z phase (black) slowly transforms into the A15 phase (pink) within 7 days at 150 °C.

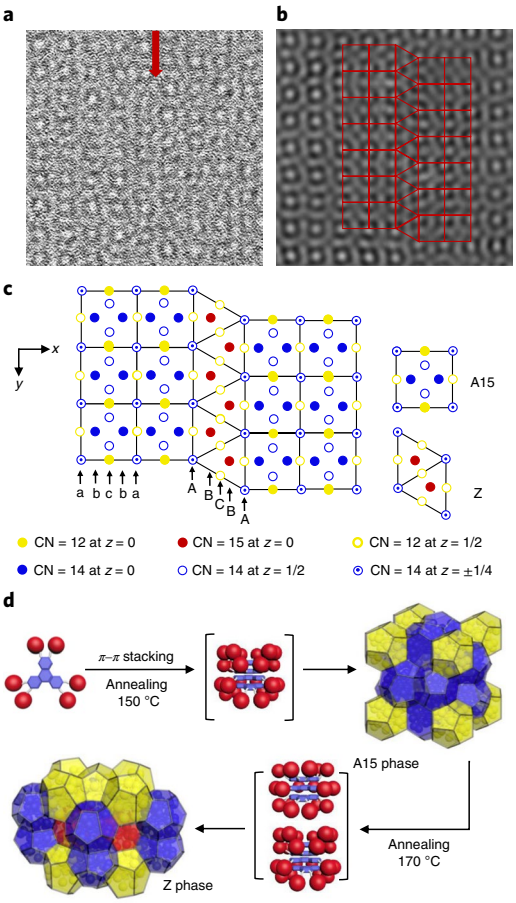

Fig. 6 | The mechanism of phase transformation. a, TEM image showing the planar defect observed during the phase transition between the A15 and Z phases (indicated by the red arrow). **b**, Fourier filtering of **a** reveals the A15 and Z lattices as marked by the red outlines. **c**, The projection is taken along [001] direction of the A15 and Z lattices. **d**, The schematic diagram illustrates the self-assembly mechanism and molecular packing in A15 and Z lattices. The coordination numbers of the yellow, blue and red polyhedra are 12, 14 and 15, respectively.

detecting range for the scattering vector from 0.01 to 0.70 Å^{-1}. The scattering vector scale was calibrated using a silver behenate standard. The typical exposure time was 0.1 s for each sample. A Linkam THMS 600 hot stage was applied to perform the in situ SAXS experiments. Laboratory SAXS data were collected from a Xeuss 2.0 equipped with a MetalJet-D2 X-ray source and Pilatus3R detector. The scattering vector scale was calibrated using a silver behenate standard. The typical exposure time was 600 s for each sample. A Mettler Toledo FPHT hot stage was used for sample annealing. All the thermal annealing processes were performed under a nitrogen atmosphere.

TEM. A JEOL-1230 TEM with an accelerating voltage of 120 kV was performed to record the bright-field images of different samples on the copper grid (300 mesh, SPI). BFTEM images were collected on a digital charge-coupled device camera. Data were processed with the accessory digital imaging system. The samples for TEM experiments were prepared by dropping 5 µl of the sample solution (1 mg ml^{-1}) onto carbon-coated copper grids. After solvent evaporation, the copper grids were annealed as in the method described above.

Data availability

The data supporting the findings of this study are available within the article and its Supplementary Information, and/or from the corresponding author upon reasonable request.

Received: 2 January 2019; Accepted: 12 August 2019;
Published online: 23 September 2019

References

1. Hyde, S. et al. *The Language of Shape: The Role of Curvature in Condensed Matter: Physics, Chemistry and Biology* (Elsevier Science, 1996).
2. Shechtman, D., Blech, I., Gratias, D. & Cahn, J. W. Metallic phase with long-range orientational order and no translational symmetry. *Phys. Rev. Lett.* **53**, 1951–1953 (1984).
3. Frank, F. C. & Kasper, J. S. Complex alloy structures regarded as sphere packings. I. Definitions and basic principles. *Acta Crystallogr.* **11**, 184–190 (1958).
4. Frank, F. C. & Kasper, J. S. Complex alloy structures regarded as sphere packings. II. Analysis and classification of representative structures. *Acta Crystallogr.* **12**, 483–499 (1959).
5. Zeng, X. et al. Supramolecular dendritic liquid quasicrystals. *Nature* **428**, 157 (2004).
6. Gillard, T. M., Lee, S. & Bates, F. S. Dodecagonal quasicrystalline order in a diblock copolymer melt. *Proc. Natl Acad. Sci. USA* **113**, 5167–5172 (2016).
7. Keys, A. S. & Glotzer, S. C. How do quasicrystals grow? *Phys. Rev. Lett.* **99**, 235503 (2007).
8. Dutour Sikiric, M., Delgado-Friedrichs, O. & Deza, M. Space fullerenes: a computer search for new Frank–Kasper structures. *Acta Crystallogr. A* **66**, 602–615 (2010).

9. Shoemaker, D. P. & Shoemaker, C. B. Concerning the relative numbers of atomic coordination types in tetrahedrally close packed metal structures. *Acta Crystallogr. B* **42**, 3–11 (1986).
10. Pauling, L. & Marsh, R. E. The structure of chlorine hydrate. *Proc. Natl Acad. Sci. USA* **38**, 112–118 (1952).
11. Baerlocher, Ch., McCusker. L. B. & Olson, D.H. *Atlas of Zeolite Framework Types* 6th edn (Elsevier Science, 2007).
12. Lin, H. et al. Clathrate colloidal crystals. *Science* **355**, 931–935 (2017).
13. Vargas, R., Mariani, P., Gulik, A. & Luzzati, V. Cubic phases of lipid-containing systems: the structure of phase Q223 (space group *Pm*3*n*). An -ray scattering study. *J. Mol. Biol.* **225**, 137–145 (1992).
14. Luzzati, V. et al. Lipid polymorphism: a correction. The structure of the cubic phase of extinction symbol *Fdc*– consists of two types of disjointed reverse micelles embedded in a three-dimensional hydrocarbon matrix. *Biochemistry* **31**, 279–285 (1992).
15. Hudson, S. D. et al. Direct visualization of individual cylindrical and spherical supramolecular dendrimers. *Science* **278**, 449–452 (1997).
16. Balagurusamy, V. S. K., Ungar, G., Percec, V. & Johansson, G. Rational design of the first spherical supramolecular dendrimers self-organized in a novel thermotropic cubic liquid–crystalline phase and the determination of their shape by X-ray analysis. *J. Am. Chem. Soc.* **119**, 1539–1555 (1997).
17. Ungar, G., Liu, Y., Zeng, X., Percec, V. & Cho, W.-D. Giant supramolecular liquid crystal lattice. *Science* **299**, 1208–1211 (2003).
18. Dukeson, D. R. et al. Application of isomorphous replacement in the structure determination of a cubic liquid crystal phase and location of counterions. *J. Am. Chem. Soc.* **125**, 15974–15980 (2003).
19. Percec, V. et al. Self-assembly of dendronized triphenylenes into helical pyramidal columns and chiral spheres. *J. Am. Chem. Soc.* **131**, 7662–7677 (2009).
20. Percec, V., Imam, M. R., Peterca, M., Wilson, D. A. & Heiney, P. A. Self-assembly of dendritic crowns into chiral supramolecular spheres. *J. Am. Chem. Soc.* **131**, 1294–1304 (2009).
21. Lee, S., Bluemle, M. J. & Bates, F. S. Discovery of a Frank–Kasper σ phase in sphere-forming block copolymer melts. *Science* **330**, 349–353 (2010).
22. Lee, S., Leighton, C. & Bates, F. S. Sphericity and symmetry breaking in the formation of Frank–Kasper phases from one component materials. *Proc. Natl Acad. Sci. USA* **111**, 17723–17731 (2014).
23. Baez-Cotto, C. M. & Mahanthappa, M. K. Micellar mimicry of intermetallic C14 and C15 laves phases by aqueous lyotropic self-assembly. *ACS Nano* **12**, 3226–3234 (2018).
24. Kim, S. A., Jeong, K.-J., Yethiraj, A. & Mahanthappa, M. K. Low-symmetry sphere packings of simple surfactant micelles induced by ionic sphericity. *Proc. Natl Acad. Sci. USA* **114**, 4072–4077 (2017).
25. Huang, M. et al. Selective assemblies of giant tetrahedra via precisely controlled positional interactions. *Science* **348**, 424–428 (2015).
26. Yue, K. et al. Geometry induced sequence of nanoscale Frank–Kasper and quasicrystal mesophases in giant surfactants. *Proc. Natl Acad. Sci. USA* **113**, 14195–14200 (2016).
27. Kim, K. et al. Thermal processing of diblock copolymer melts mimics metallurgy. *Science* **356**, 520–523 (2017).
28. Kim, K. et al. Origins of low-symmetry phases in asymmetric diblock copolymer melts. *Proc. Natl Acad. Sci. USA* **115**, 847–854 (2018).
29. Zhang, W.-B. et al. Molecular nanoparticles are unique elements for macromolecular science: from 'nanoatoms' to giant molecules. *Macromolecules* **47**, 1221–1239 (2014).
30. Zhang, W. et al. Sequence-mandated, distinct assembly of giant molecules. *Angew. Chem. Int. Ed.* **56**, 15014–15019 (2017).
31. Reddy, A. et al. Stable Frank–Kasper phases of self-assembled, soft matter spheres. *Proc. Natl Acad. Sci. USA* **115**, 10233–10238 (2018).
32. Date, R. W. & Bruce, D. W. Shape amphiphiles: mixing rods and disks in liquid crystals. *J. Am. Chem. Soc.* **125**, 9012–9013 (2003).
33. Glotzer, S. C. Some assembly required. *Science* **306**, 419–420 (2004).
34. Osawa, T. et al. Wide-range 2D lattice correlation unveiled for columnarly assembled triphenylene hexacarboxylic esters. *Angew. Chem. Int. Ed.* **51**, 7990–7993 (2012).
35. Vorländer, D. Die Erforschung der molekularen Gestalt mit Hilfe der kristallinischen Flüssigkeiten. *Z. Phys. Chem.* **105**, 211–254 (1923).
36. Wilson, C. G., Thomas, D. K. & Spooner, F. J. The crystal structure of Zr_4Al_3. *Acta Crystallogr.* **13**, 56–57 (1960).
37. Ishimasa, T. & Fukano, Y. Planar defect in A15 structure observed in Cr–Si fine particles. *Jpn J. Appl. Phys.* **22**, 1092–1097 (1983).
38. Arita, M. & Nishida, I. Defects of A15 small particles in tungsten thin films. *Surf. Rev. Lett.* **3**, 1191–1194 (1996).
39. Ziherl, P. & Kamien, R. D. Maximizing entropy by minimizing area: towards a new principle of self-organization. *J. Phys. Chem. B* **105**, 10147–10158 (2001).

Acknowledgements

This work was supported by National Science Foundation (DMR-1408872 to S.Z.D.C. and CHE-1808115 to C.W.) and the Program for Guangdong introducing Innovative and Entrepreneurial Teams (no. 2016ZT06C322). This research used resources of the Advanced Photon Source, a US Department of Energy (DOE) Office of Science User Facility operated for the DOE Office of Science by Argonne National Laboratory under contract no. DE-AC02-06CH11357. T. L. is grateful to the support by the Northern Illinois University start-up funds.

Author contributions

Z.S., M.H. and S.Z.D.C. designed the project. Z.S., Z.G. and J.H. synthesized and characterized the samples. J.M. and C.W. contributed to the matrix-assisted laser desorption/ionization mass experiments. Z.S., X.F., T.L. and S.S. carried out the SAXS experiments. Z.S. and R.Z. carried out the TEM experiments. Z.S., C.-H.H., W.Z., T.A., S.Z.D.C. and Y.W. analysed the data. Z.S., M.H. and S.Z.D.C. wrote the paper.

Competing interests

The authors declare no competing interests.

Additional information

Supplementary information is available for this paper at https://doi.org/10.1038/s41557-019-0330-x.

Correspondence and requests for materials should be addressed to M.H. or S.Z.D.C.

Reprints and permissions information is available at www.nature.com/reprints.

Publisher's note Springer Nature remains neutral with regard to jurisdictional claims in published maps and institutional affiliations.